

Capturing the Stratosphere's Influence on Seasonal and Intraseasonal Predictability in a State-of-the-Art Navy Global Environmental Model (NAVGEN)

Stephen D. Eckermann
Geospace Science & Technology Branch
Code 7631, Space Science Division
Naval Research Laboratory
Washington DC 20375

Phone: (202) 404-1299 Fax: (202) 404-7997 email: stephen.eckermann@nrl.navy.mil

Award Number: N0001412WX21321
<http://www.nrl.navy.mil/ssd/>

LONG-TERM GOALS

Recent research has revealed that the stratosphere influences medium- and long-range weather prediction, sometimes strongly (NAS 2010). The North Atlantic Oscillation (NAO) – one of the most prominent modes of intraseasonal tropospheric variability extending from the subtropical Atlantic to the Arctic (Hurrell et al. 2003) – has been recognized only within the past decade as one regional manifestation of a larger hemispheric phenomenon, known synonymously as the Arctic Oscillation (AO) or Northern Annular Mode (NAM). The NAM extends continuously into the stratosphere and mesosphere, and an analogous deep Southern Annular Mode (SAM) occurs in the southern hemisphere. NAM/SAM anomalies often appear first in the upper stratosphere or mesosphere, then descend gradually over a period of weeks, sometimes reaching the surface where they change weather patterns throughout the polar region (Baldwin and Dunkerton 2001; Coy et al. 2011). Descending stratospheric NAM/SAM anomalies also play a pivotal role in controlling the response of high-latitude weather to the El-Niño/Southern Oscillation in the tropics (Bell et al. 2009; Ineson and Scaife 2009), while the tropical stratosphere and mesosphere may also impact tropical seasonal prediction through an improved Madden-Julian Oscillation (Weare et al. 2012). These examples, and others like them, point to the important role that the overlying stratosphere-mesosphere system can play in presaging and regulating large-scale global surface weather changes over periods of weeks to months (e.g., Baldwin et al. 2003), prompting recent reports from the World Climate Research Programme (WCRP 2008) and the National Academy of Sciences (NAS 2010) that note (quote) “*the stratosphere’s potential to improve seasonal forecasts is largely untapped.*”

Thus the long-term goals of this project are to tap the potential of an improved stratosphere and mesosphere for seasonal prediction by developing and testing new stratospheric and mesospheric modeling, prediction and data assimilation capabilities, all specifically designed to improve long-range prediction capabilities of the Navy Global Environmental Model (NAVGEN).

OBJECTIVES

The overarching objective of this proposal is to gain an improved understanding of how the stratosphere and mesosphere in a state-of-the-art numerical weather prediction (NWP) system affect

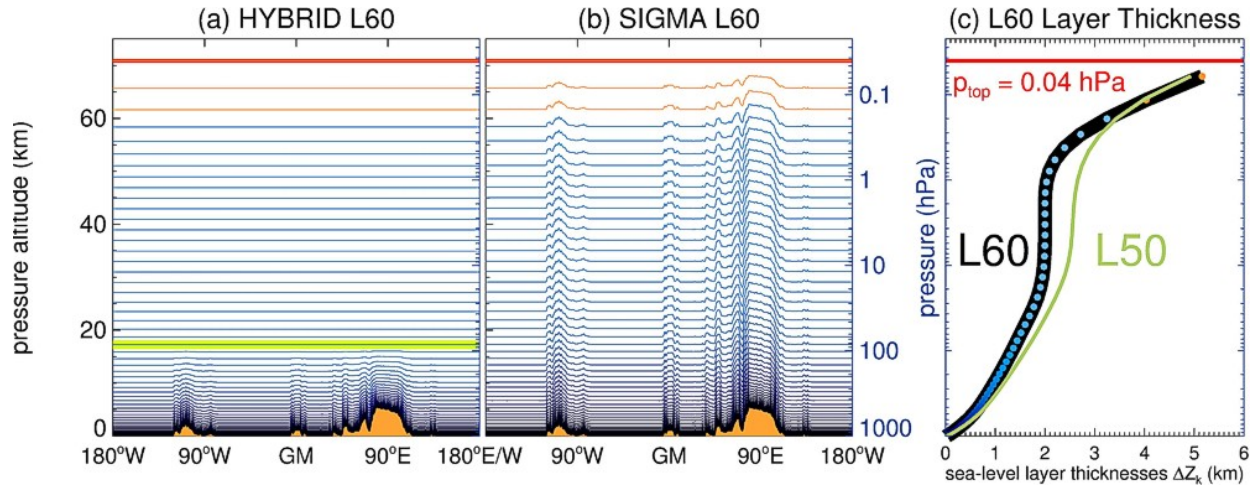


Figure 1. New NAVGEM L60 vertical levels plotted around a $34.5^{\circ}N$ latitude circle using the (a) NEWHYB2 hybrid σ - p vertical coordinate of Eckermann (2009) and (b) the terrain-following σ coordinate. The green line in (a) shows the lowest isobaric interface layer at ~ 85 hPa. The red curve shows the rigid upper boundary of 0.04 hPa (~ 70 km). The pressure height thicknesses ΔZ_k for a sea-level surface pressure of 1013.25 hPa are plotted in (c) for the L60 layers (black, blue dots) and are compared to the corresponding profile for the older NAVGEM L50 levels (green curve). Note in (c) the improved L60 vertical resolution throughout the troposphere and stratosphere.

atmospheric prediction on time scales from days to months. To achieve this, our research focuses on the following scientific questions:

1. What are the fundamental dynamics and dominant physical coupling pathways governing the stratosphere-troposphere interaction that are most relevant for atmospheric prediction on time scales from days to months?
2. Which physical and dynamical processes in the forecast model are important in controlling this deep vertical coupling, and how sensitive is forecast skill to details in their numerical implementation?

APPROACH

Our primary tool is NAVGEM, the Navy’s next-generation NWP system, comprising a new semi-Lagrangian (SL) global forecast model coupled to the four-dimensional variational (4DVAR) NRL Atmospheric Variational Data Assimilation System – Accelerated Representer (NAVDAS-AR). Our approach to utilizing NAVGEM for this research is guided by the following recommendations of WCRP (2008) and NAS (2010) to address knowledge gaps in our current understanding of coupled troposphere-stratosphere predictability:

- R1. Models *must* extend to *at least* 0.01 hPa (~ 80 km altitude) with a full range of appropriate physical parameterizations, so as to properly predict stratospheric and mesospheric variability;

R2. Research should then focus on the extended system’s ability to reproduce and delineate the poorly understood connections between stratospheric and tropospheric circulations.

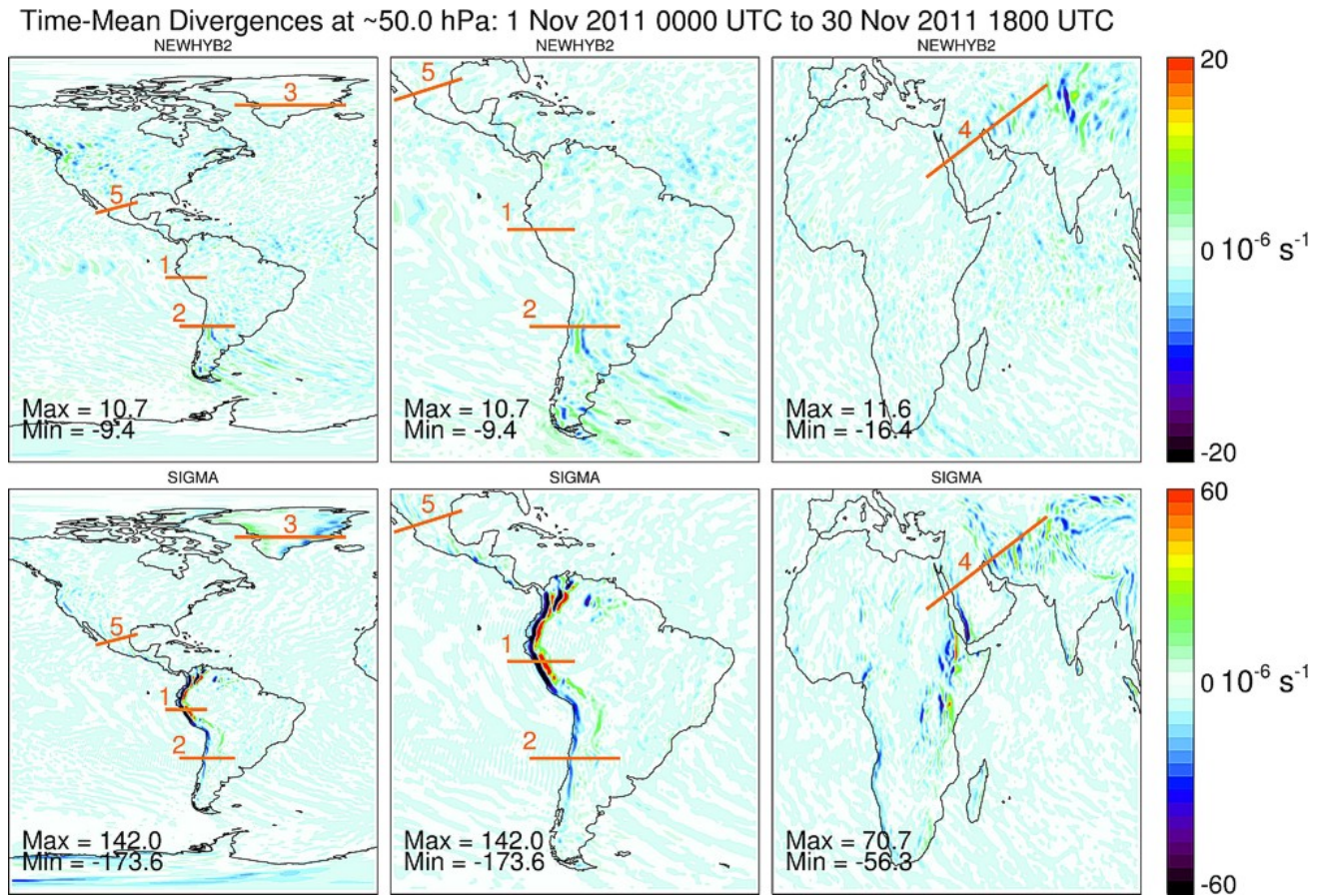


Figure 2. Maps of time-mean analyzed NAVGEM 50-hPa divergences for November 2011 on the NAVGEM model grid over different land masses, for the HYB experiment (top row) and the SIG experiment (bottom row). Note the lower dynamic range of the color scale (far right) for the HYB experiment relative to SIG. Maximum and minimum values (units 10^{-6} s^{-1}) are shown at bottom-left of each panel. Orange curves show 5 cross sections profiled in Figure 3 of Eckermann et al. (2013) and discussed in the text.

R1 Tasks

To address R1, our project is progressively augmenting the NAVGEM SL forecast model and DAS in ways that improve its ability to predict the integrated troposphere-stratosphere-mesosphere system, as outlined in tasks (a)-(e) below. These tasks are described, justified and linked scientifically in detail in the original science proposal.

- (a) SL model tests using additional vertical layers and resolution
- (b) Improved radiative heating and cooling rates for the SL model’s stratosphere and mesosphere
- (c) Improved ozone and water vapor photochemistry for the upper stratosphere and mesosphere
- (d) Parameterizations of subgrid-scale gravity-wave drag for the stratosphere and mesosphere
- (e) Assimilation of stratospheric and mesospheric satellite observations

R2 Tasks

To address R2, we perform the following component tasks using the augmented NAVGEM model, as progressively developed via successful execution of the R1 tasks listed above. Again, these tasks are described and scientifically motivated in significant detail in the original science proposal.

- (a) Bias identification and parameterization correction/improvement
- (b) Forecast-assimilation experiments supporting international research projects on predictability
- (c) Realistic tropical QBO (quasi-biennial oscillation) and SAO (semiannual oscillation)
- (d) Prediction of stratospheric sudden warmings (SSWs) and stratospheric NAM/SAM anomalies
- (e) Tropospheric influences of stratospheric NAM/SAM anomalies
- (f) Tropospheric coupling to the stratospheric QBO

WORK COMPLETED

Task R1a. (leads: Steve Eckermann, Jim Ridout). This year we replaced the operational NAVGEM L50 vertical levels with a new L60 formulation that improved vertical resolution throughout the troposphere and stratosphere, as shown in Figure 1c. This new T359L60 NAVGEM configuration is currently undergoing preoperational testing for potential FY14 transitions to FNMOC.

To research how NWP skill is affected by the vertical coordinate, we used this new T359L60 NAVGEM to perform two forecast-assimilation experiments that were identical apart for the form of the vertical coordinate. As illustrated in Figure 1, one experiment (HYB: see Figure 1a) used the hybrid σ -p vertical coordinate of Eckermann (2009), which smoothly transitions vertical model layers from terrain-following surfaces near the ground to isobaric (constant pressure) surfaces above a lower stratospheric interface layer (shown in green in Fig. 1a) at ~ 85 hPa. The second experiment (SIG: Fig. 1b) used the standard terrain-following σ coordinate throughout the domain. These experiments were motivated by some paradoxical results in the literature concerning stratospheric forecast and analysis skill using hybrid and sigma coordinates, reviewed by Eckermann et al. (2013).

Our research has clarified the origins of this confusion and has demonstrated, unambiguously and for the first time, that the hybrid coordinate not only reduces model error growth, but leads to statistically significant improvements in stratospheric skill scores. This work was written up and recently accepted for publication in Monthly Weather Review (Eckermann et al. 2013).

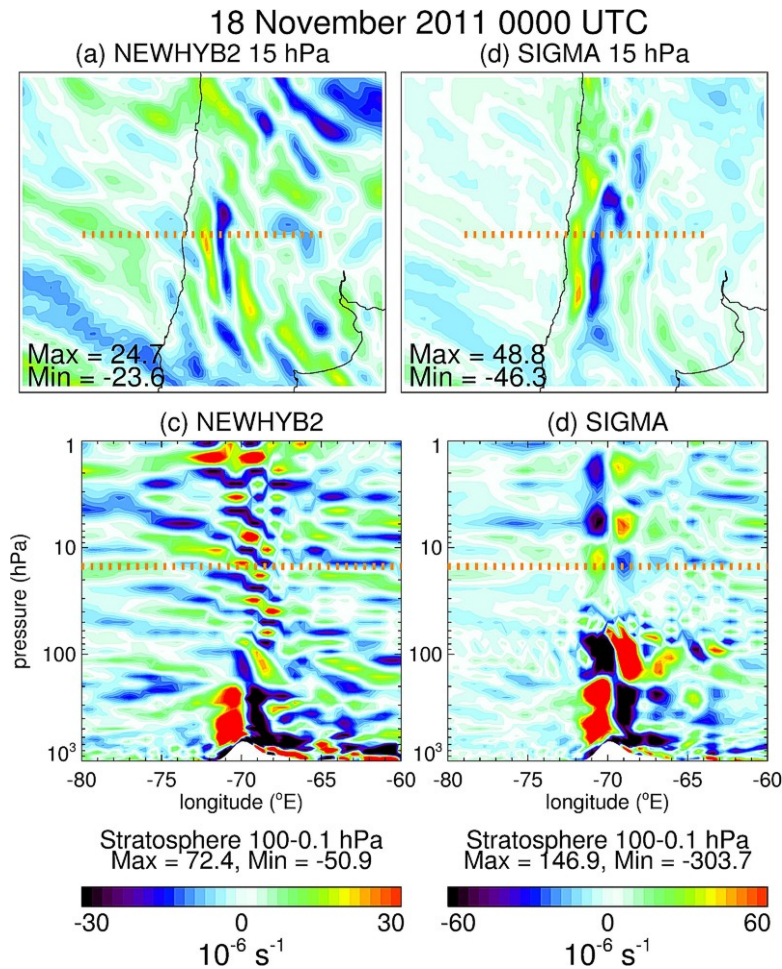


Figure 3. Maps of analyzed NAVGEM divergence at 15 hPa on 18 November 2011 at 0000 UTC over the Andes for the (a) HYB and (b) SIG experiment. Dotted orange line shows cross section at 30°S, along which longitude-height cross sections of divergence are plotted in the panels beneath. Maximum and minimum stratospheric values are given beneath each panel.

Our first major research finding, summarized in Figure 2, was that the stratospheric analyses in the NAVGEM SIG experiment produced large mean anomalies in wind divergence fields over regions with high steep terrain, whereas these anomalies were essentially absent from corresponding analysis fields produced by the NAVGEM HYB experiment. This anomalous structure in the SIG experiment directly above terrain is very similar to unexplained wind anomalies reported by Trenberth and Stepaniak (2002) in NCEP/NCAR reanalyses (see their Figs. 5 and 6). In particular, vertical cross sections along the orange lines in Fig. 2 (not shown here, but see Fig. 3 of Eckermann et al. 2013) show an oscillating anomalous divergence structure in the SIG analyses extending from the surface to the model top. Eckermann et al. (2013) demonstrate that these anomalies can be explained as model discretization errors in the computation of pressure gradient forces on model layers tilted by steep underlying terrain, which can amplify considerably in the stratosphere due to the sharp change in the vertical gradient in temperature at the tropopause (Eckermann 2009).

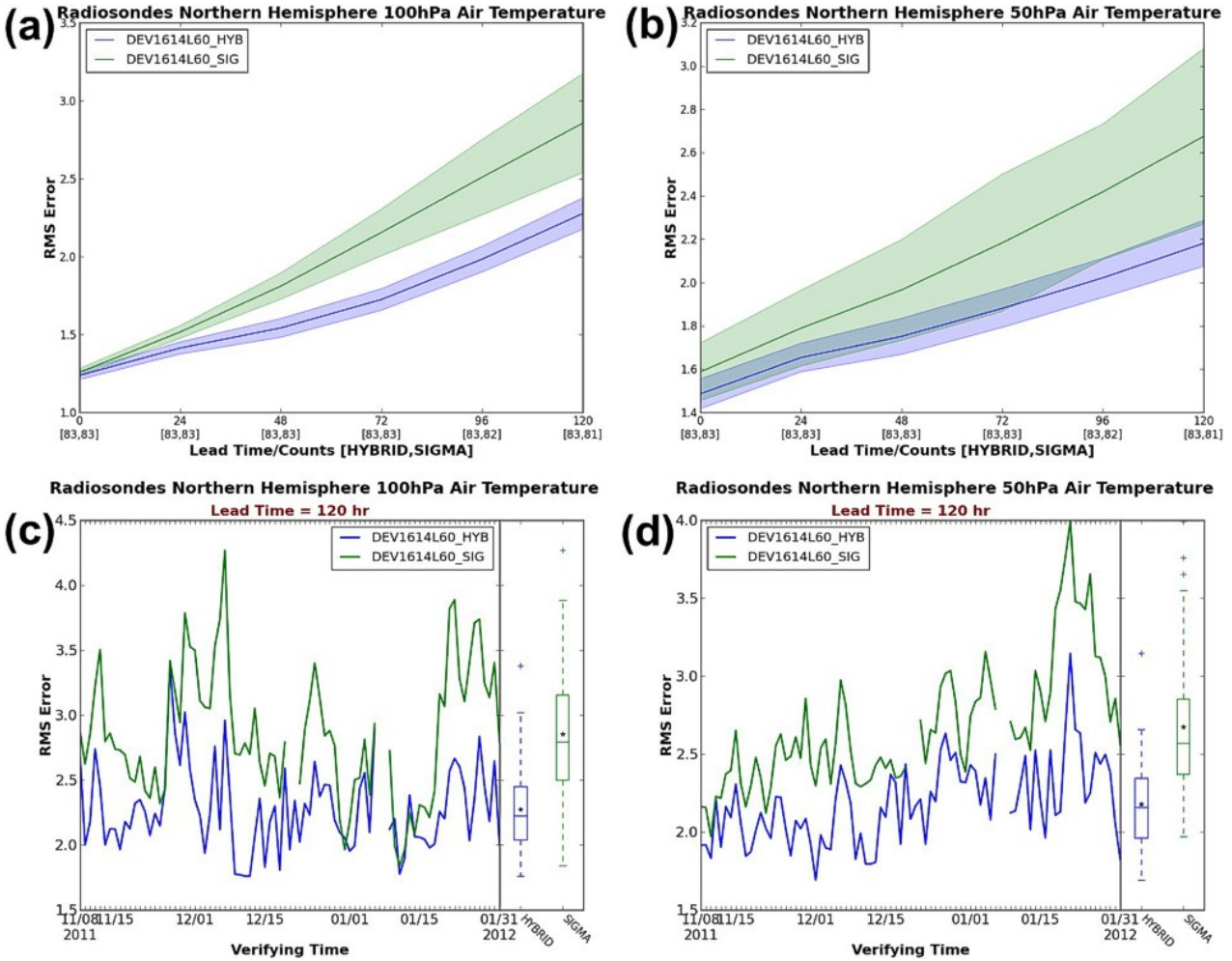


Figure 4. Plots of mean rms temperature error (with respect to radiosondes) versus forecast hour, averaged from 8 November 2011 to 31 January 2012 at (a) 100 hPa and (b) 50 hPa for experiments SIG (green) and HYB (purple). Solid line is mean and shaded area denotes standard deviation. Bottom row shows corresponding time series of 120 hour forecast errors at (c) 100 hPa and (d) 50 hPa, with mean whisker plot statistics on right of each panel.

Figure 3 provides an example of how these anomalous deep divergence structures above steep terrain in the SIG experiments degrade analysis skill. The top panels of Fig. 3 show maps of analyzed 15 hPa divergences from the HYB and SIG experiments, which both appear to capture plane orographic gravity-wave structure emanating from the Andes below. However, corresponding longitude-height cross sections at $\sim 30^\circ\text{S}$ in the panels beneath show that only the HYB analysis captures a realistically tilted gravity-wave phase structure throughout the troposphere and stratosphere, whereas the SIG cross section is dominated by standing-wave-like anomalies due to deep model discretization errors.

Daily 0–120 hour forecasts from each NAVGEM experiment were used to quantify forecast skill over the entire analysis period, excluding the initial “spin up” period from 5 October 2011 to 7 November 2011. Top panels of Figure 4 plot the root-mean-square (rms) temperature errors versus forecast hour at 100 hPa and 50 hPa in the Northern Hemisphere averaged over the period 8 November 2011 to 31

January 2012, using radiosondes as verification. Panels below show corresponding time series of these rms temperature errors at 120 hours. Persistent and statistically significant differences are evident, with the HYB experiment consistently outperforming the SIG experiment in stratospheric skill scores. Other results (not shown) reveal improved 50 hPa and 100 hPa skill in the tropics, in other fields such as winds, and when using self-analysis rather than radiosondes as verification (see Eckermann et al. 2013 for further details).

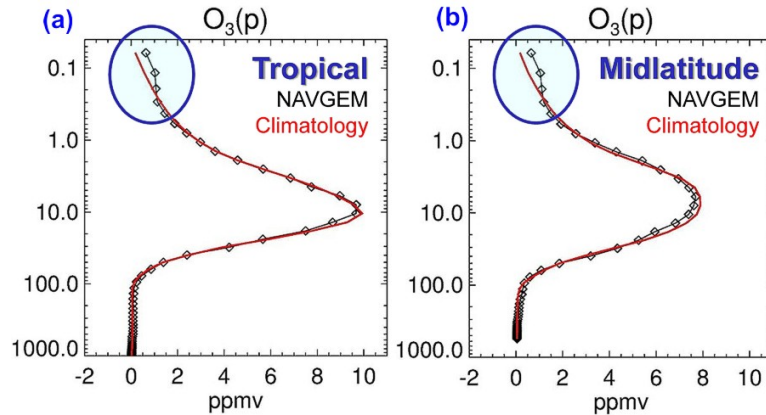


Figure 5. Profiles of NAVGEM prognostic ozone mixing ratios (ppmv) versus height (given in atmosphere pressure hPa) plotted as black curves and symbols, compared to observational climatology (red curves) at an (a) tropical and (b) midlatitude grid point. Note the excessive ozone mixing ratios at upper levels in the lower mesosphere.

Tasks R1b and R1c. (leads: Steve Eckermann, John McCormack). The research for these two tasks merged this year due to the strong coupling between radiation and chemistry in the stratosphere and mesosphere. Our work was motivated by some persistent NAVGEM cold biases in the lower stratosphere that could be related in part to: (a) excessive lower stratospheric water vapor that gives rise to too much infrared radiative cooling and (b) excessive ozone at upper levels (Fig. 5) that leads to excessive shortwave ozone absorption and heating at upper levels, leaving reduced solar UV fluxes at lower altitudes and thus insufficient ozone heating at lower levels. Both issues point to potential errors in NAVGEM’s prognostic water vapor and ozone fields that require attention, which may in turn improve radiative heating rates at all NAVGEM levels down to the surface and improve the cold bias problem.

Figure 6 shows an example of this water vapor research. Figure 6a plots zonal-mean water vapor specific humidities q from NAVGEM analysis on 20 November 2011 at 0000 UTC. Below it, Figure 6c shows the corresponding zonal-mean observational climatology of specific humidity for November. Comparison of the two plots reveals substantial moisture differences in the stratosphere and mesosphere. At upper levels the NAVGEM analyzed q values are too low, whereas in the Southern Hemisphere above the tropopause from altitudes ~ 300 -40 hPa the NAVGEM values are too large.

In efforts to rectify these moisture biases, we have developed a significantly upgraded version of the NRL water vapor chemistry scheme of McCormack et al. (2008). The new scheme uses updated photochemical equilibrium states and chemical production and loss rates, and also includes a new quality control (QC) option that incorporates accelerated photochemical destruction of large stratospheric water vapor outliers that the earlier linearization approach was ill-equipped to handle. This QC code produces a smooth increase in the photochemical relaxation rate in proportion to the

288-Hour NAVGEM Forecasts: November 2011

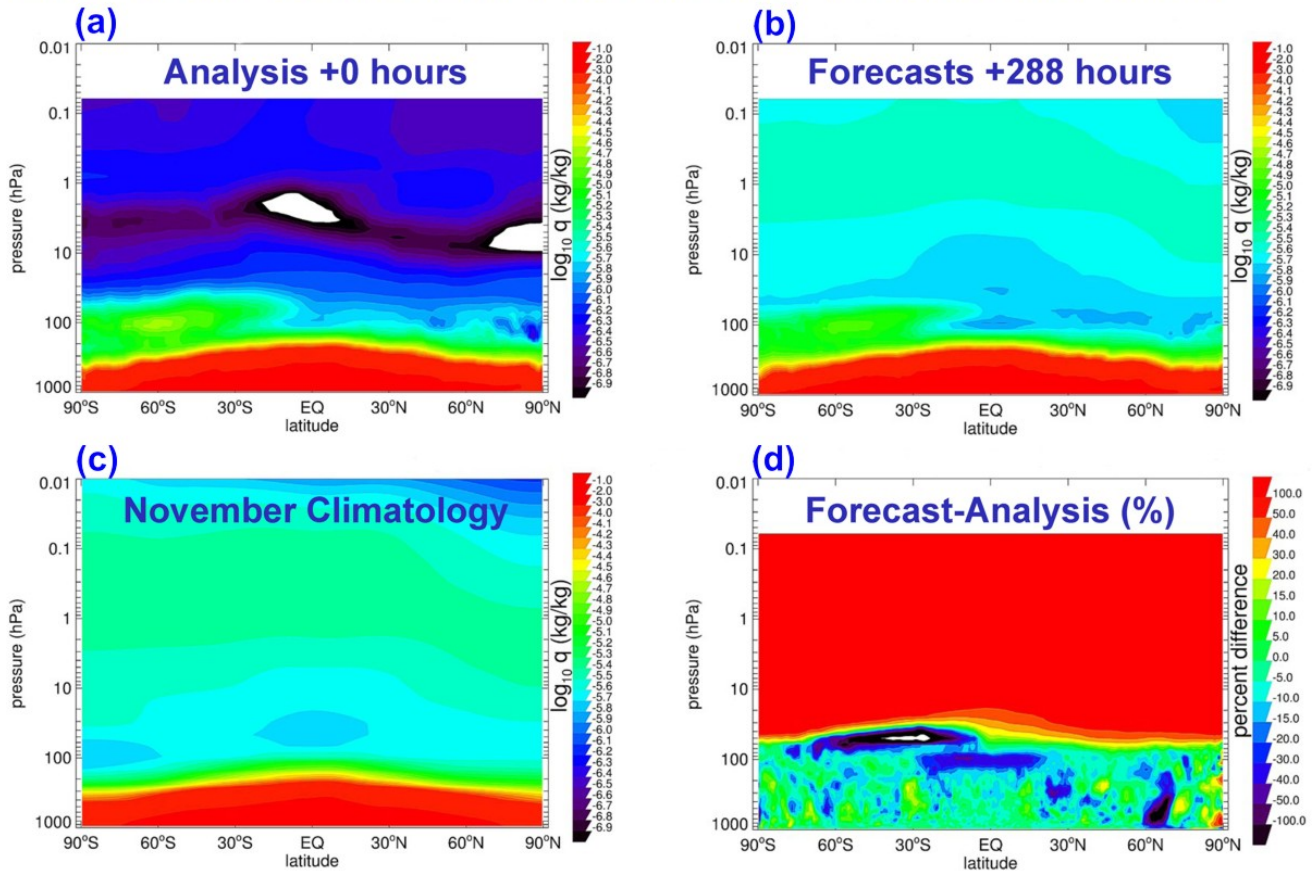


Figure 6. Zonal mean specific humidity q (kg/kg, color bars show $\log q$ values) for November 2011 versus altitude (pressure hPa) and latitude from (a) NAVGEM analysis, which shows large biases at upper levels with respect to the observation climatology in (c). Panel (b) shows prognostic humidity after 288 hours from a NAVGEM forecast with new water vapor chemistry and humidity QC, which substantially improves moisture levels from 50-0.1 hPa but still retains moist biases just above the tropopause. See text for further details.

deviation of local water vapor from photochemical equilibrium values: high moisture outliers are rapidly photochemically destroyed, low moisture outliers are rapidly replenished through production via methane oxidation. The new code has been extensively tested in the single column model, was ported to NAVGEM and tested (see below), and is currently in the process of being fully intergrated into the developmental NAVGEM code for use by NRL's entire NAVGEM development team.

Figure 6b shows zonal-mean specific humidity from a 288 hour NAVGEM forecast initialized on 20 November 2011 using this new water vapor chemistry and QC code. The chemistry is activated only at levels above 80 hPa in this particular run. We see that the new chemistry code substantially improves the moisture values from 80 hPa all the way up the model top (c.f. Figs. 6b and 6a), making them moister and far more consistent with observational climatologies (c.f. Figs. 6b and 6c). However, Fig. 6b also shows that, at altitudes below 80 hPa where the new water vapor chemistry and QC is deactivated, the lower stratospheric high moisture biases remain. In this “middle world” between the troposphere and stratosphere, there is a combination of moist tropospheric cloud processes and

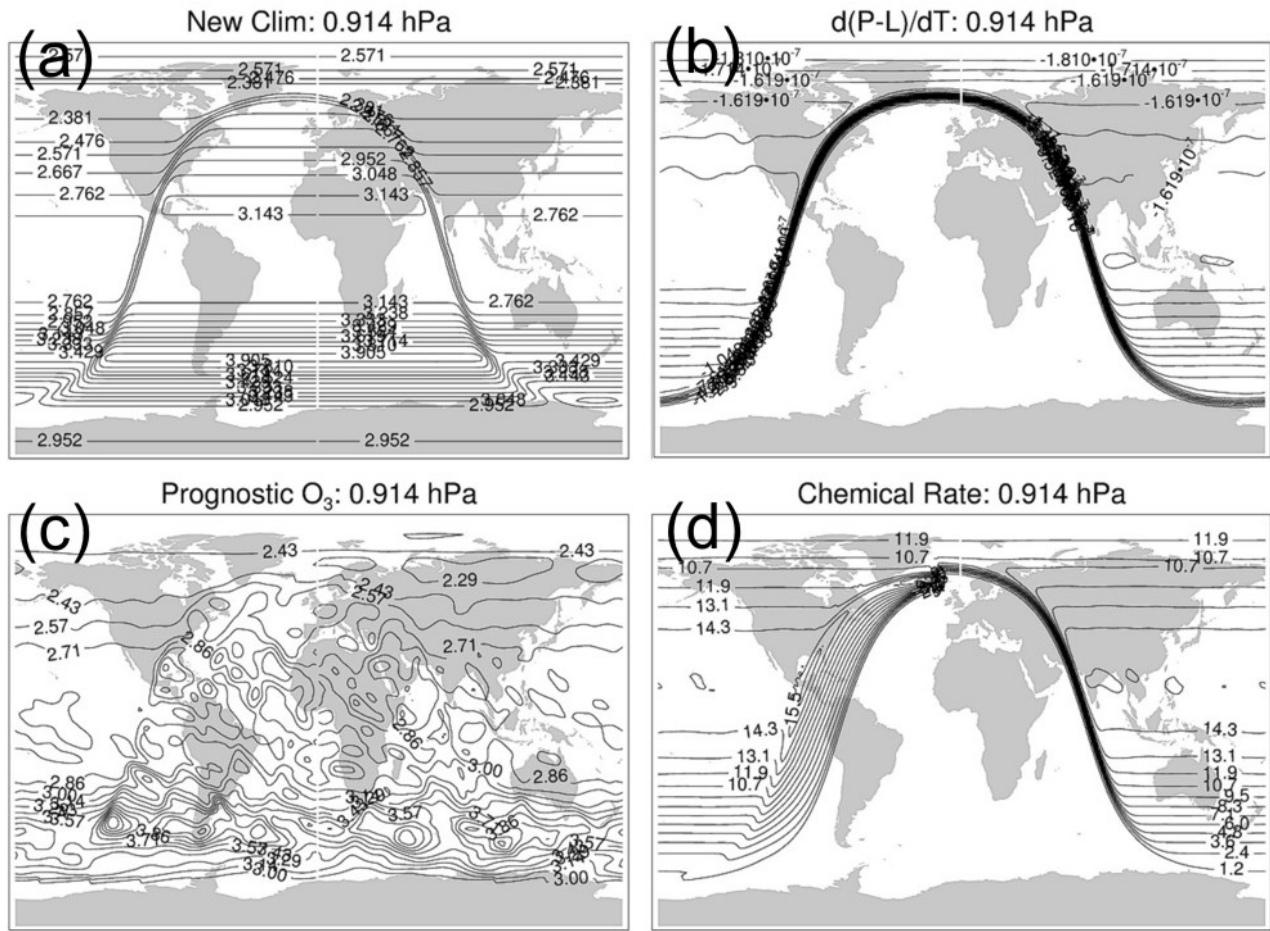


Figure 7. Instantaneous global maps at 0.914 hPa of (a) equilibrium ozone concentration (ppmv), (b) temperature dependent photochemical rate coefficient (ppmv $K^{-1} s^{-1}$), (c) prognostic ozone (ppmv), and (d) photochemical damping rate (days $^{-1}$), using the new NRL ozone photochemistry of Eckermann and McCormack (2013).

stratospheric chemistry processes, and it is important that the two processes do not compete unrealistically against one another's tendencies. Consequently, given the initial successes noted in Figure 6, we are now working on a more sophisticated scheme that restricts the photochemical and QC parameterization to operate ~ 1 -2 km above the diagnosed tropopause, in efforts to eliminate these lower stratospheric moist biases while at the same time not negatively impacting tropospheric cloud physics parameterizations.

For ozone, the high ozone biases at upper levels in Figure 5 originate from shortcomings in the current NRL ozone photochemistry parameterization of McCormack et al. (2006), which is based on an equilibrium diurnal-mean odd-oxygen chemistry whose assumptions begin to break down above ~ 50 km altitude. At upper levels monatomic oxygen O rather than ozone dominates odd-oxygen chemistry, so that the ozone photochemical time scale becomes short as it responds quickly to larger changes in O. These changes give rise to diurnal variations in ozone and a modified daytime and nighttime chemistry that yields much larger ozone concentrations at night compared to the day. Consequently we have generalized the NRL parameterized odd-oxygen chemistry of McCormack et al. (2006) to include a height dependent partition ratio of monatomic oxygen to ozone concentrations, $\Lambda=[O]/[O_3]$, that

tracks the transition from the stratosphere, where ozone is the major odd oxygen constituent, to the mesosphere and lower thermosphere (MLT) where O dominates. This leads to Λ -dependent perturbations to the diurnal mean linearized photochemical coefficients that increase with height. These are scaled by a new gridpoint parameter ε_d , representing the fraction of the day that is sunlit (specified for efficiency using a seasonally varying global lookup table), which acts to convert the previous diurnal-mean ozone photochemical coefficients into daytime values. We next include an entirely new nighttime ozone photochemistry, which is based on the equilibrium recombination model of Allen et al. (1984), and requires specification of a vertical profile of the ozone night-to-day ratio which we take from a detailed offline photochemistry calculation. Finally, these separate daytime and nighttime photochemical coefficients must be carefully combined across the terminator using a zenith-angle dependent interpolation, along with a localized photochemical rate increase near the terminator to mimic rapid chemical recombination just after sunset. Complete details are given in Eckermann and McCormack (2013).

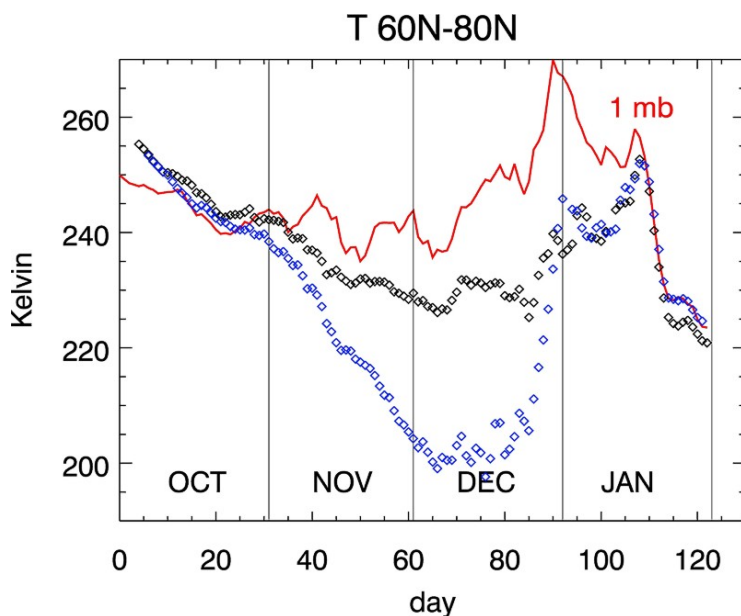


Figure 8. Time series of analyzed NAVGEM temperatures (K) at 60°-80°N versus time (1 October 2011 to 10 February 2012) at 1 hPa (~48 km altitude) for a control run (blue symbols) and another run that includes the new unified gravity-wave drag scheme (black symbols). Observed temperatures from the Microwave Limb Sounder on NASA's Aura satellite are plotted in red.

The new scheme has been preliminarily tested in a new global offline NAVGEM simulator. This extension from a single column model to a global simulator proved necessary here to test the new complex zenith-angle dependence of the new chemistry. Figure 7 shows an example of these tests, revealing the large day-night differences in the ozone chemistry now introduced into this new scheme. These include larger photochemical equilibrium ozone concentrations at night relative to day (Fig. 7a), and temperature-dependent modifications to the daytime rates that disappear at night (Fig. 7b) due to a long tracerlike chemical behavior at night relative to the day (Fig. 7d). Fig. 7d also reveals the fast rates during the day, the accelerated rate due to recombination just after sunset, and long tracerlike rates at night. These and other chemical processes combine to give the final prognostic ozone field in Fig. 7c. Fig 7c reveals new realistic features of these ozone solutions, including significant small-scale variability at night due to dynamical perturbations that are not removed by the slow nighttime

chemistry, compared to daytime where the fields are smoother due to photochemical rates that are faster and tend to photochemically damp slower dynamical perturbations to the ozone concentrations.

The new chemistry is slated for integration into the NAVGEM SL model pending the successful initial transition of the water vapor scheme, upon which this more complex ozone chemistry update builds. We plan further work on this scheme during FY14 with a view to improving the coupled chemistry and radiation budgets, which in turn should help in reducing stratospheric temperature biases.

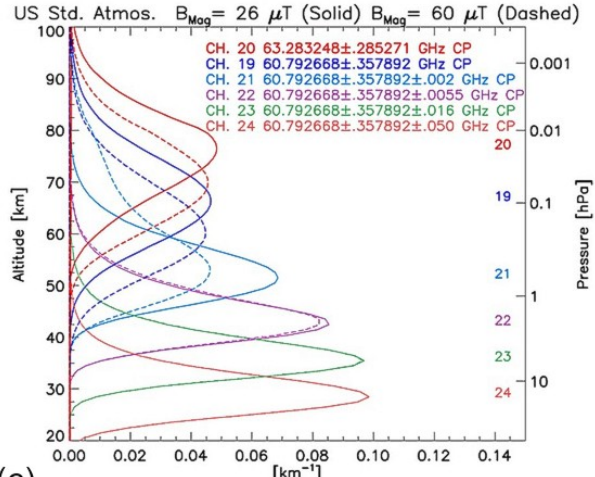
Task R1d. (leads: Steve Eckermann, John McCormack) Leveraging research funded under the “Parameterizations” DRI (Award No. N0001411WX21220, see Year 3 report), this year we preliminarily integrated a new unified gravity-wave drag parameterization code coming out of that research work into NAVGEM, and have begun testing its impacts on NAVGEM prediction skill. It should be noted that we believe the thermal budget work just discussed above under Tasks R1b-R1c is important to make further progress on prior to detailed integration of this scheme, since all of these gravity-wave drag schemes must be tuned to some extent, and it is important that this tuning takes place within the context of a model with an accurate thermal radiation budget.

Figure 8 shows an example of some preliminary NAVGEM forecast-assimilation experiments that we have conducted this year with this new gravity-wave drag parameterization included. The blue curves show mean analyzed temperatures averaged from 60°-80°N from a control NAVGEM T359L60 run without the new parameterized gravity-wave drag. The actual temperatures observed at this time and altitude are plotted in red, and were derived from independent research observations from the Microwave Limb Sounder (MLS) on NASA’s Aura satellite. The blue and red curves reveal a substantial cold bias in the analyzed NAVGEM stratospheric temperatures in boreal winter. The black curves in Figure 8 show the results from a corresponding T359L60 NAVGEM run which included the new unified gravity wave drag parameterization. This NAVGEM run with gravity-wave drag included (black curve in Figure 8) produces a substantially improved 1 hPa temperature analysis relative to the control (blue curve) that immediately and substantially improves the cold bias with respect to the independent MLS Aura observations (red curve). It is clear that the scheme is already having immediate large positive impacts on NAVGEM prediction skill in the upper stratosphere. This scheme was also implemented and tuned in another developmental NAVGEM used to assimilate SSMIS UAS radiances, as described below under Task R1e (see Hoppel et al. 2013).

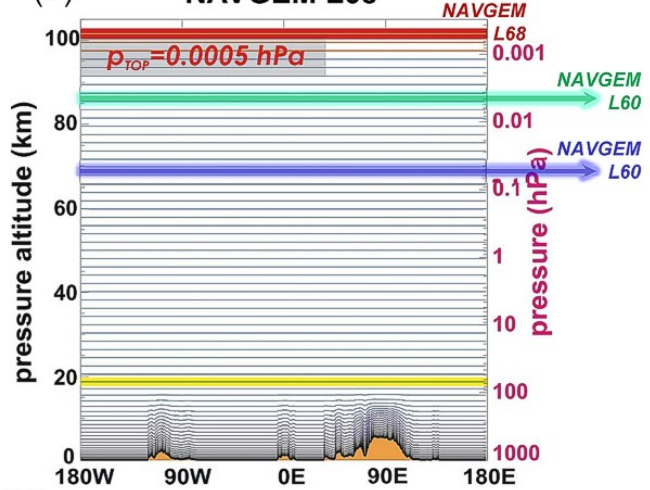
Task R1e. (leads: Karl Hoppel, Steve Eckermann). This work was extensively documented in last year’s report, and this year we completed the major research work under this task, leading to a writeup of these world-first results that has just been published in the peer-reviewed scientific literature (Hoppel et al. 2013). A brief summary of this research work is provided below, as full details are contained in the journal article.

As illustrated in Figures 9a and 9b, we configured a high-altitude NAVGEM prototype to assimilate upper atmosphere sounding (UAS) channel radiances acquired by the Special Sensor Microwave Imager/Sounder (SSMIS) currently operating on the operational F16, F17 and F18 satellites of the Defense Meteorological Satellite Program (DMSP). The time periods and local-time sampling of each of the 3 orbiting SSMIS sensors is shown in Fig. 9d, while the typical geographical sampling is shown in Fig. 9c. Radiances from the 6 SSMIS UAS channels are acquired from atmospheric emissions from narrow spectral bands located near line centers of the O₂ magnetic dipole transitions. As a result, the VWFs of these UAS channel radiances are significantly affected by the Zeeman interaction of the

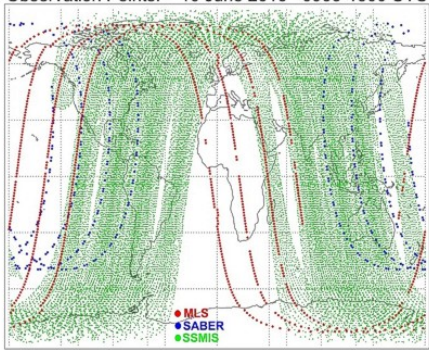
(a) SSMIS UAS Nadir Weighting Functions



(b) NAVGEM L68



(c) Observation Points: 10 June 2010 0900-1500 UTC



(d) Polar Orbiter Equatorial Crossing Times

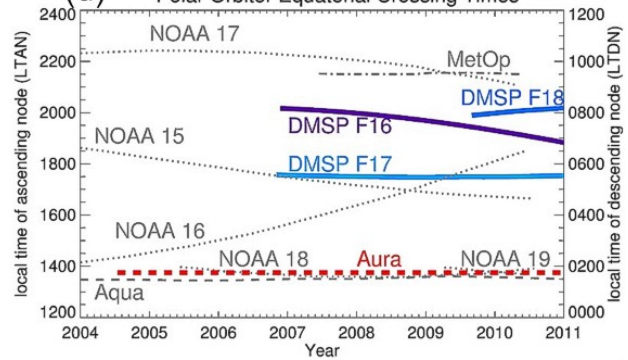


Figure 9. (a) SSMIS UAS vertical weighting functions for a weak geomagnetic field typical of equatorial regions (solid curves) and for a strong magnetic field typical of polar regions leading to Zeeman splitting of the O_2 microwave lines (dashed curves). (b) altitude coverage of the extended L60 and L68 NAVGEM configurations used for SSMIS assimilation relative to the standard L60 shown in Figure 1. (c) MLT measurement locations for MLS (red), SABER (blue) and SSMIS on DMSP F16, F17 and F18 (green) on 10 June 2010 from 0900-1500 UTC. (d) sampling of the DMSP (blue/purple), Aura (red) and other operational sensors (gray) as a function of year and local time of the ascending node (LTAN) of equatorial crossing. See text and Hoppel et al. (2013) for further details.

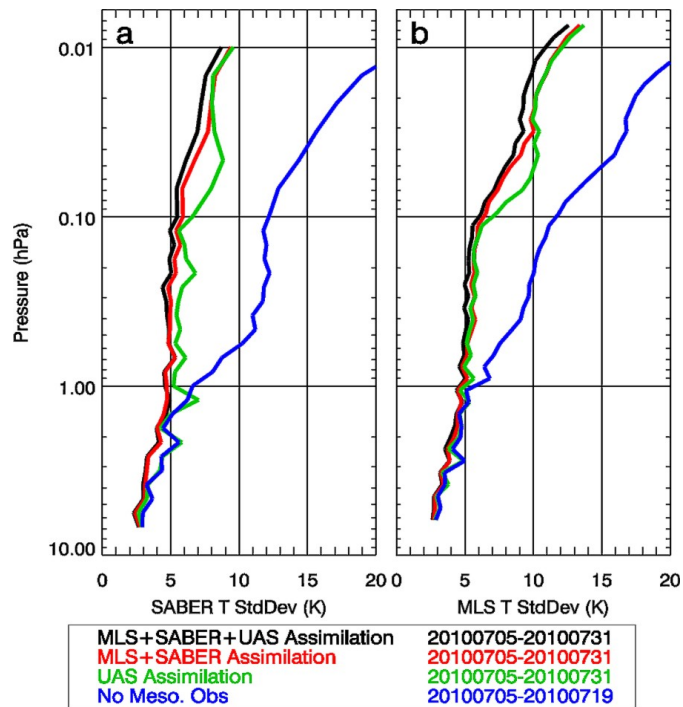


Figure 10. Standard deviation of observations minus forecasts for NAVGEM experiments assimilating no MLT observations (blue), SSMIS UAS radiances (green), SABER and MLS temperatures (red) and SABER, MLS and UAS observations (black). The observational comparisons use (a) SABER and (b) MLS temperatures (after Hoppel et al. 2013).

O₂ molecule's electronic spin with the Earth's magnetic field, as well as by Doppler shifts due to the rotation of the Earth (c.f. solid and dotted curves in Fig. 9a). To accurately assimilate the temperature information contained in these radiances, we integrated into NAVGEM the latest fast radiative transfer model of Han et al. (2007, 2010), which accounts for these physical processes in the forward modeling component of the radiance assimilation, with new geophysical inputs of the geomagnetic field vector and the SSMIS antenna pointing direction. Our experiments also assimilated MLT temperature measurements from the MLS and SABER sensors on NASA research satellites. We performed 4 different forecast-assimilation experiments to better understand and benchmark the impacts on analysis and forecast skill of our SSMIS UAS assimilation. Those experiments were: (a) a control run with no SSMIS, MLS or SABER assimilation; (b) a run that assimilated SSMIS radiances; (c) a run that assimilated MLS and SABER data, and; (d) a run that assimilated the SSMIS, MLS and SABER observations.

The results of these experiments revealed that the assimilation of SSMIS UAS radiances into NAVGEM yielded upper-level temperature analyses that were comparable in skill to experiments assimilating data from the research-grade MLS and SABER sensors, and which substantially improved upper-level analysis and prediction skill. A series of results were shown in last year's report and more detail is provided in Hoppel et al. (2013). One example is shown in Figure 10, which shows how the SSMIS UAS NAVGEM assimilation experiment (green) substantially reduces temperature standard deviation errors with respect to the control experiment (blue), and also gives very similar reduced errors to experiments that assimilate research observations from MLS and SABER (black and red curves).

In the upcoming year we are planning to transition this new SSMIS radiance assimilation capability into the developmental NAVGEM code repository so that it is available for testing by the entire NRL NAVGEM development community, with a view to possible transitions to FNMOCC.

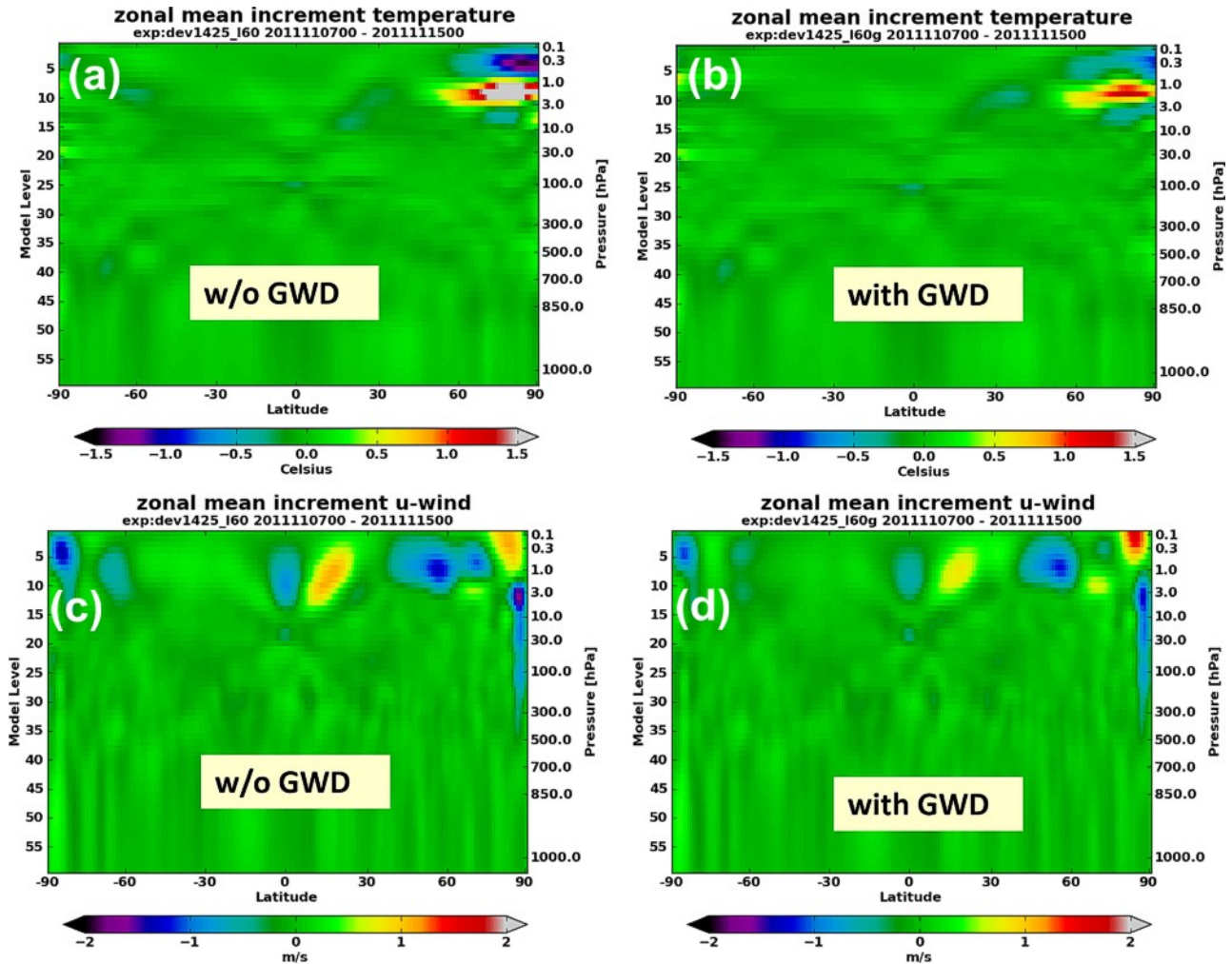


Figure 11. Zonal-mean temperature increments versus NAVGEM model level (left axis, pressure on right axis) and latitude averaged over 7-15 November 2011 for T359L60 NAVGEM update cycle experiments. Results are shown for temperature (top row) and zonal winds (bottom row) for a control experiment without gravity-wave drag (left) and a corresponding experiment that includes the new gravity-wave drag parameterization from Task R1d (right), which reduces observational increments everywhere relative to the control.

RESULTS

Task R2a. (leads: Karl Hoppel, Doug Allen, Steve Eckermann). This year, the tasks R1c, R1d and R1e were all focused on parameterization improvements that reduced apparent temperature biases at upper levels identified in this task (see Figs. 8 and 10). In particular, the integration of SSMIS thermal radiances into NAVGEM through the successful completion of Task R1e yielded new observations

that allowed observational increments from the NAVGEM data assimilation phase to be used for objective identification of mean temperature and wind biases in the forecast model.

Figure 11 provides an example of this bias identification using the mean observational increments. The panels on the left show temperature and zonal wind increments from a control NAVGEM run without the new gravity-wave drag parameterization from Task R1d. The corresponding results on the right come from the NAVGEM run with the new gravity-wave drag parameterization included, and show substantial reductions in both upper-level temperature and zonal wind increments, both at high latitudes and in the tropics, consistent with the reduced wind and temperature biases produced by these gravity-wave drag circulations (c.f. Fig. 8). This new upper-level incrementing procedure enabled by the assimilation of UAS data in Task R1e automates to some extent the objective identification and correction of bias in the forecast model, and represents substantial progress in this Task.

Task R2b. (lead: Steve Eckermann). Our modeling tasks supporting the international Stratospheric Network on Assessment of Predictability (SNAP) of the World Climate Research (<http://www.sparcsnap.org/>) were put substantially behind schedule this year due to the cancellation of all international conference and workshop travel by NRL scientists during FY13. As a result, NRL was unable to attend or contribute to the pivotal SNAP kickoff workshop in Reading, England in April 2013 where experiments were planned and schedules put into place (note: remote attendance through VTEL/sharegroups was also denied due to security concerns). Our absence led to a series of experiment choices and timetables that proved to be impossible for NRL to commit to, especially given reduced manpower (due to unreplaced staff due to federal hiring freeze and 4-day furloughs in late FY13). A follow-on teleconference call is planned for 7 October 2013 at which NRL will be represented, during which time we hope to make representations that enable us to contribute runs to SNAP within the current manpower, computing and funding we are operating under. We hope to begin to make better progress in this task during FY14, after the October SNAP telecon, and hopefully within a more stable federal operating environment for such work.

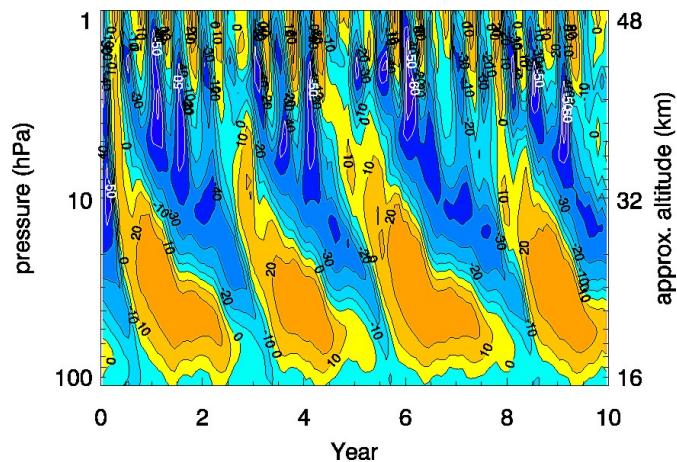


Figure 12. Mean zonal winds ($m s^{-1}$, red/yellow is eastward, blue is westward) from $5^{\circ}S-5^{\circ}N$ from a 10-year nature run at T79L139 using stochastic gravity-wave drag parameterization with reduced vertical mixing and a new tropical wave source (McCormack and Eckermann 2013). Note the quasi-two-year QBO-like wind oscillation in the lower stratosphere and the realistic SAO at higher altitudes.

Task R2c. (lead: John McCormack). We made changes to the gravity-wave drag parameterization and various other properties of the global model that eventually enabled us to generate a realistic self-consistent quasi-biennial oscillation (QBO) and tropical semiannual oscillation (SAO) in the model winds. The necessary changes to achieve this were: (a) increasing the vertical resolution in the stratosphere to ~500m; (b) producing a small tropical enhancement in parameterized gravity-wave momentum flux; (c) changing the dominant horizontal wavelength of the parameterized tropical gravity waves from 100 km to 700 km (after Hurwitz et al. 2010); (d) reducing the horizontal spectral diffusion in the stratosphere, and; (e) preventing the vertical diffusion due to the planetary boundary layer mixing parameterization from activating in the stratosphere. We also activated the stochastic (fast) form of the gravity-wave drag parameterization. In a 10-year T79L139 nature run, the model was able to reproduce without additional tuning a very realistic QBO in lower stratospheric tropical winds, with a realistic period of ~28 months and realistic descending easterly and westerly QBO shear zones. Furthermore, above these QBO winds the nature run also reproduced a realistic upper stratospheric SAO. It should be noted that neither feature could be simulated at all prior to these changes, so this represents a major breakthrough in the model's seasonal prediction capabilities. We have started writing these research results up with a view to submitting them to the peer-reviewed scientific literature (McCormack and Eckermann 2013).

Tasks R2d & R2e. (leads: Steve Eckermann, Carolyn Reynolds). As noted in last year's report, we have made significant research progress in diagnosing the role of evolving stratospheric NAM/SAM anomalies on deep troposphere-stratosphere coupling during Arctic winter. Considerable progress was made by noting for the first time that the fast-growing stratospheric perturbations during stratospheric sudden warming (SSW) events, as diagnosed using the leading singular vectors (SVs) of the flow (SV1, SV2, etc.), were characterized by global NAM-like structures that had a major role in either enhancing (+SV1) or reducing (-SV1) the intensity of the forecast SSW, as well as of the descending NAM anomalies that potentially impact the Arctic surface weather some time later. An example derived during this year's research is shown in Figure 13, which plots difference maps, with respect to a control forecast, of forecast zonal-mean zonal winds after addition (+SV1, top row) and subtraction (-SV1, bottom row) of the leading stratospheric SV associated with rapid perturbation growth during the SSW. As the figures show, both the +SV1 and -SV1 perturbations lead, respectively, to weakened (blue) or strengthened (red) stratospheric westerlies with respect to the unperturbed control forecast, which develop in the stratosphere after 24 hours and then, over the forecast period, both intensify and descend to impact surface winds in the high-latitude Arctic. This is a convincing objective demonstration of how stratospheric perturbation growth is affecting tropospheric weather through rapidly growing and descending NAM-like circulation anomalies.

The initial results of this work were reviewed in last year's report and were written up and accepted for publication in the peer-reviewed scientific literature this year (Coy and Reynolds 2013). This year we have been engaged in deeper dives into the fundamental dynamics controlling this perturbation growth and the larger dynamical consequences for predictability and skill, leading to new results such as those shown in Figure 13. We are currently studying particle trajectories in and around these growing perturbation zones to understand the perturbation dynamics here better in terms of Lyapunov exponents and lobe dynamics. We are also studying the dynamics of these events in greater detail, using isentropic potential vorticity maps to study the three-dimensional dynamics of the wave breaking that seed early perturbation growth, as well as the fundamental dynamical mechanisms that initially support growth of these perturbations.

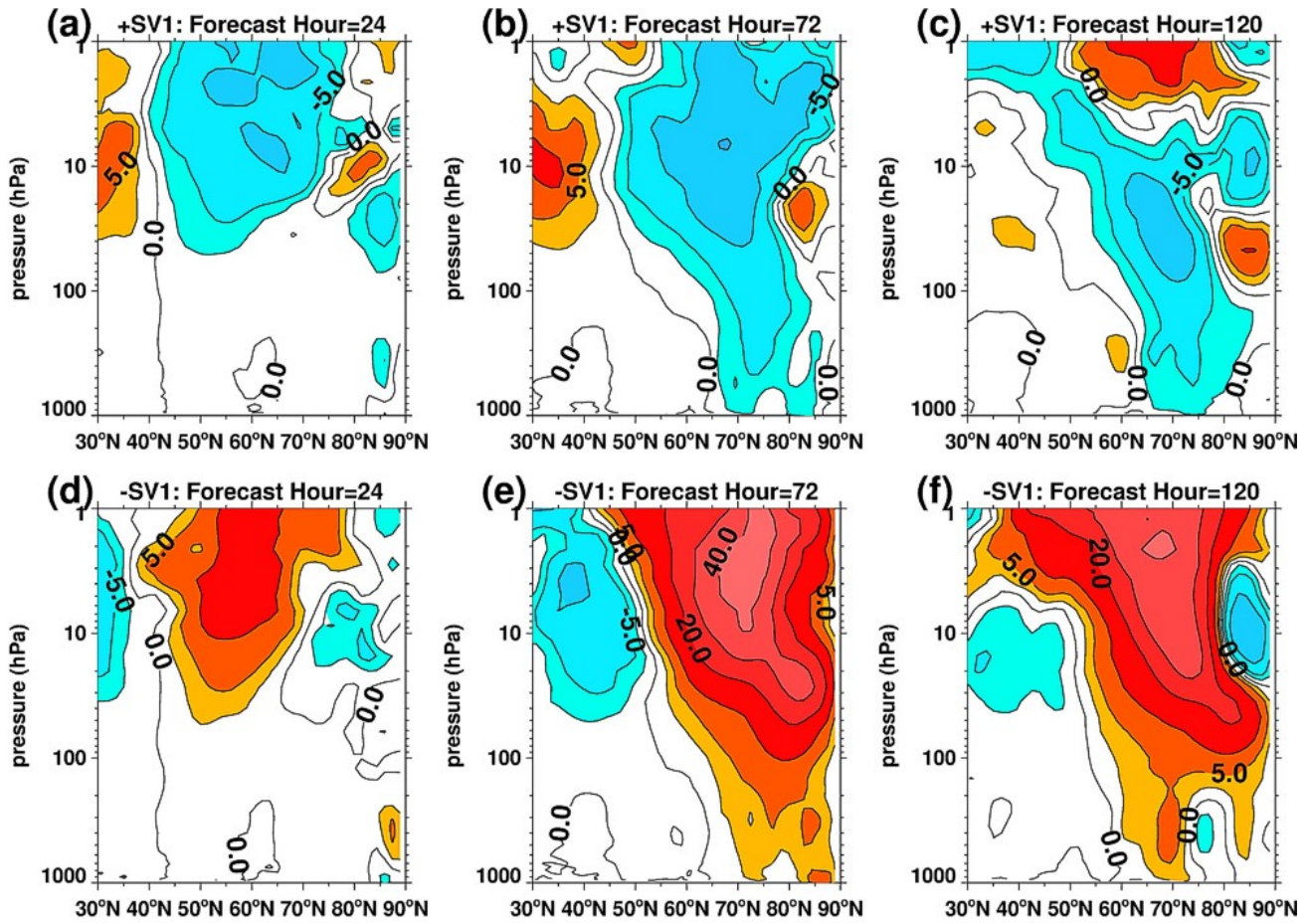


Figure 13. Latitude-height cross sections of zonal-mean zonal wind perturbations derived as differences between (top row) +SV1-perturbed and control, and (bottom row) -SV1-perturbed and control forecasts initialized on 22 January 2009 at 0000 UTC. Wind speed contours are 2.5 m s^{-1} , 5 m s^{-1} , 10 m s^{-1} and at 10 m s^{-1} intervals thereafter, with blue/red contours depicting easterlies/westerlies. Results are shown for the (left) 24 hour, (middle) 72 hour, and (right) 120 hour forecasts.

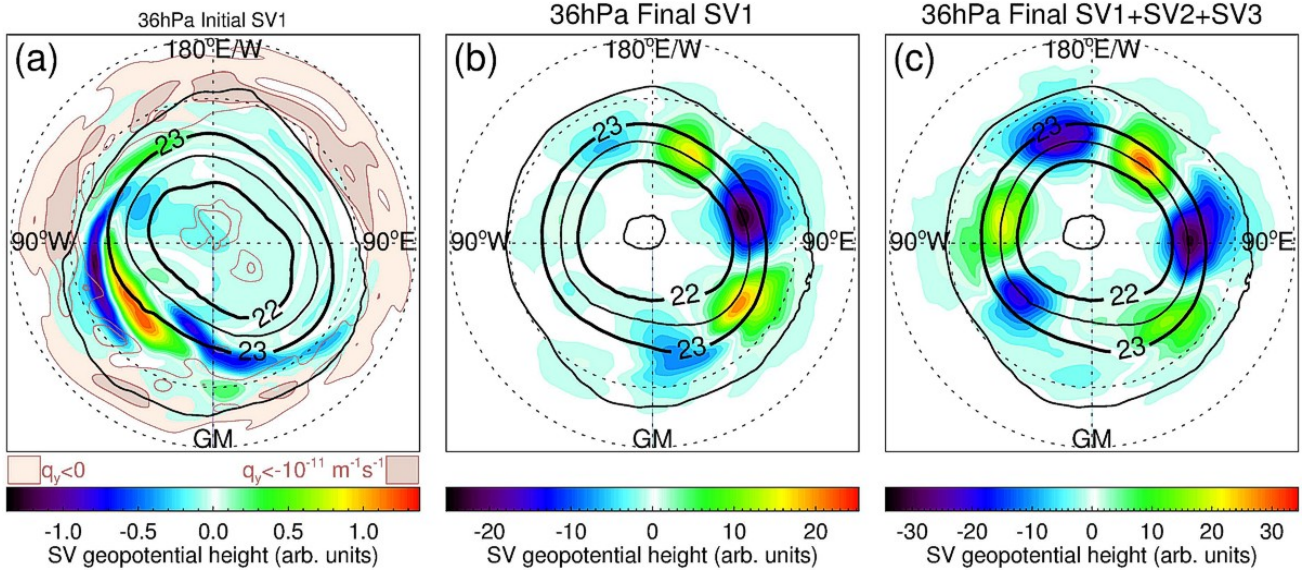


Figure 14. Polar orthographic plots of geopotential height SV perturbations at 36 hPa from the stratospheric NP4t6 SV experiment initialized on 7 January at 0000 UTC: (a) initial SV1, (b) final (+72 hour) SV1 and (c) final (+72 hour) SV1-SV3 perturbations (arbitrary units, see color bars). Black contours show 30 hPa geopotential heights from the forecast (contour labels in km). Beige-shaded contours in (a) show 30 hPa regions of negative q_y computed from eq. (1).

One example of this dynamical research is shown in Figure 14, where the colored perturbations show the initial SV1 (Fig. 14a) and final SV1 (Fig. 14b) and SV1-3 (Fig. 14c) of the 36 hPa geopotential height perturbations initialized on 7 January 2009 at 0000 UTC. The initial perturbations form in Fig. 14a as highly tilted structures near the extremities of the stratospheric vortex, then evolve and grow over time into untilted wave-3 Rossby-wave trains riding along the peak vortex wind regions in Figs. 14b-14c. Why do initial perturbations form where they do? To study this, we computed meridional gradients in the quasi-geostrophic potential vorticity q , evaluated as

$$q_y = \frac{\partial q}{\partial y} = \frac{\partial \zeta}{\partial y} - \frac{f^2}{\rho} \frac{\partial}{\partial z} \left[\rho N^{-2} \frac{\partial u}{\partial z} \right] \quad (1)$$

where ζ is the absolute vorticity, f is the inertial frequency, N^2 is static stability, ρ is density, u is zonal wind, y is meridional displacement and z is pressure altitude. Beige contours in Fig. 14a show regions where q_y in (1) is negative, implying inertially unstable wind gradients supporting rapid perturbation growth in exactly the regions where initial SV1 perturbations are found to grow in the forecast model. This implies a well-defined “surf zone” of unstable gradients at the edge of the vortex preconditioned by earlier wave breaking events that provides a background environment amenable to strong polar focusing of planetary waves that subsequently drive the SSW (e.g., McIntyre 1982).

Our research on the fundamental dynamics of these growing modes will continue next year with a view to a second dynamics-focused publication on this topic in the peer-reviewed scientific literature. **Tasks R2f.** (lead: John McCormack). With the progress in both our QBO and SSW modeling (Tasks R2c-R2e), we have begun to research some of the potential complex dynamical coupling pathways

linking tropospheric responses to the QBO. We performed ensembles of 120-day nature runs during the boreal winter period of 2008. One set of ensembles used the forecast model with an ability to simulate the QBO as in Figure 12 (using the gravity-wave drag parameterization) and the other set of ensembles deactivated the tropical gravity-wave drag, so that the model produced no internal QBO or SAO.

In the ensemble of runs containing the QBO, equatorial stratospheric winds were westerly throughout the winter, consistent with observations for the 2007-2008 winter. In the ensemble of runs without the QBO, weak easterly flow persisted in the equatorial stratosphere throughout the winter. Ensemble mean differences in sea level pressure (SLP) over the Arctic during March, plotted in Figure 15, show lower polar cap SLP and higher mid-latitude SLP when the QBO is included in the model. White contours enclose regions where these SLP differences are statistically significant at the 99% confidence level. The results in Fig. 15 demonstrate that the westerly phase of the QBO acts to reinforce the positive high-latitude NAM teleconnection pattern throughout boreal winter that penetrates all the way to the surface. The result reveals a statistically significant coupling between NAM-like SLP anomalies in the Arctic and the QBO of the tropical stratosphere, which is an important new finding. The dynamics of these teleconnection pathways continue to be researched using these forecast runs.

Δ SLP (QBO - NO QBO) : 200803

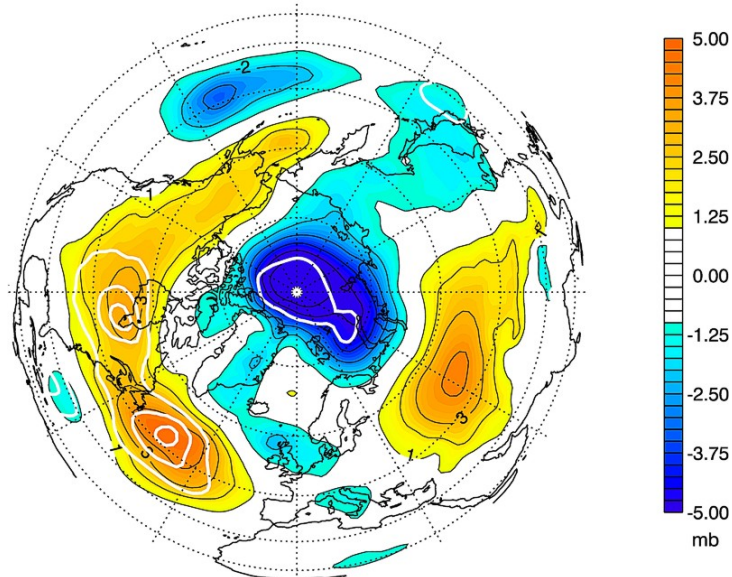


Figure 15. Ensemble-mean Arctic SLP differences (hPa, see color bar on right) for March 2008 between QBO and non-QBO forecast model runs. White contours enclose SLP contours that are significant at >99%.

IMPACT/APPLICATIONS

The Oceanographer of the Navy (Naval Meteorology and Oceanography Command: CNMOC) has selected NAVGEM to be the Navy's bridging technology from its existing NWP capability at the time (NOGAPS) to a future Earth System Prediction Capability (ESPC) predicting the atmosphere seamlessly across time scales from days to decades. The improved NAVGEM seasonal prediction capabilities provided by this project are moving the Navy closer to a future operational ESPC

generating ensemble forecasts on a continuum of time scales spanning weather and climate. Specifically, improved models of deep stratosphere-troposphere coupling provided by this research are improving NAVGEM's ability to predict deeply coupled regional weather events and systems that are highly relevant for seasonal prediction problems of direct relevance to Navy operations. The salient phenomena, such as Arctic sea ice movement and extent, severe Arctic temperature anomalies, gale-force oceanic winds and high ocean-wave conditions, are all potentially affected, possibly majorly, by deep vertical coupling of NAM/SAM anomalies from the stratosphere to the surface (e.g., Thompson et al. 2002). The research work performed under this project is directly targeting improvements in NAVGEM that will allow it to model and predict these features more accurately and out to longer lead times (weeks to months).

TRANSITIONS

We transitioned a series of new code options to the NAVGEM “trunk” and “development” code repositories, including new L60 vertical layers (Fig. 1), initial SSMIS UAS data assimilation code, and the new water vapor photochemistry and QC code. The gravity-wave drag parameterization code is currently in the process of preparation for imminent transition to the developmental NAVGEM in early FY14, with the new ozone photochemistry code to follow it soon thereafter.

RELATED PROJECTS

Doyle, J. D., and S. D. Eckermann, *The Boundary Paradox*, NRL 6.1 Accelerated Research Initiative, 1 October 2010-30 September 2015.

Eckermann, S. D, and collaborators, *New Approaches to the Parameterization of Gravity-Wave and Flow-Blocking Drag due to Unresolved Mesoscale Orography Guided by Mesoscale Model Predictability Research*, ONR Award Number: N0001411WX21220, 1 October 2011-30 September 2014.

Hoppel, K. W., *High Altitude Data Assimilation for NWP*, NRL 6.2 Work Unit, 1 October 2009-September 2013.

REFERENCES

- Allen, M., J. Lunine, and Y. Yung (1984), The vertical distribution of ozone in the mesosphere and lower thermosphere, *J. Geophys. Res.*, 89, 4841–4872.
- Baldwin, M. P., and T. J. Dunkerton (2001), Stratospheric harbingers of anomalous weather regimes, *Science*, 244, 581–584.
- Baldwin, M.P., D.B. Stephenson, D.W.J. Thompson, T.J. Dunkerton, A.J. Charlton, A. O'Neill (2003), Stratospheric memory and extended-range weather forecasts, *Science*, 301, 636-640.
- Bell, C. J., L. J. Gray, A. J. Charlton-Perez, M. M. Joshi, and A. A. Scaife (2009), Stratospheric communication of El Niño teleconnections to European winter. *J. Climate*, 22, 4083–4096.
- Coy, L., and C. A. Reynolds (2013), Structure and evolution of stratospheric singular vectors during the January 2009 stratospheric sudden warming, *Quart. J. Roy. Meteorol. Soc.*, in press.
- Coy, L., S. D. Eckermann, K. W. Hoppel, and F. Sassi (2011), Mesospheric precursors to the major stratospheric sudden warming of 2009: Validation and dynamical attribution using a ground-to-

edge-of-space data assimilation system, *J. Adv. Model. Earth Syst.*, 3, M10002, 7pp., doi:10.1029/2011MS000067.

- Eckermann, S. D. (2009), Hybrid σ -p coordinate choices for a global model, *Mon. Wea. Rev.*, 137, 224-245.
- Eckermann, S. D. (2011), Explicitly stochastic parameterization of nonorographic gravity-wave drag, *J. Atmos. Sci.*, 68, 1749-1765.
- Eckermann, S. D., K. W. Hoppel, L. Coy, J. P. McCormack, D. E. Siskind, K. Nielsen, A. Kochenash, M. H. Stevens, C. R. Englert, and M. Hervig (2009), High-altitude data assimilation system experiments for the northern summer mesosphere season of 2007, *J. Atmos. Sol.-Terr. Phys.*, 71, 531-551.
- Eckermann, S. D. and J. P. McCormack (2013), Extension of linearized parameterizations of gas-phase stratospheric ozone photochemistry through the upper stratosphere, mesosphere and lower thermosphere, (paper in preparation).
- Han, Y, et al. (2007), A fast radiative transfer model for SSMIS upper atmosphere sounding channels. *J. Geophys. Res.*, 112, D11121, doi:10.1029/2006JD008208.
- Han, Y., P. van Delst, and F. Weng (2010), An improved fast radiative transfer model for special sensor microwave imager/sounder upper atmosphere sounding channels. *J. Geophys. Res.*, 115, D15109, doi:10.1029/2010JD013878.
- Hoppel, K. W., N. L. Baker, L. Coy, S. D. Eckermann, J. P. McCormack, G. E. Nedoluha, and D. E. Siskind (2008), Assimilation of stratospheric and mesospheric temperatures from MLS and SABER into a global NWP model, *Atmos. Chem. Phys.*, 8, 6103-6116.
- Hoppel, K. W., S. D. Eckermann, L. Coy, G. E. Nedoluha, D. R. Allen, S. D. Swadley, and N. L. Baker (2013), Evaluation of SSMIS upper atmosphere sounding channels for high-altitude data assimilation, *Mon. Wea. Rev.*, 141, 3314-3330.
- Hurrell, J.W., Y. Kushnir, G. Ottersen, and M. Visbeck (2003), *The North Atlantic Oscillation: Climate Significance and Environmental Impact*, AGU Geographical Monograph Ser. 134, 279pp.
- Hurwitz, M. M., P. Braesicke, and J. A. Pyle (2011), Sensitivity of the mid-winter Arctic stratosphere to QBO width in a simplified chemistry-climate model. *Atmosph. Sci. Lett.*, 12: 268-272. doi: 10.1002/asl.330.
- Ineson, S., and A. A. Scaife (2009), The role of the stratosphere in the European climate response to El Niño, *Nat. Geosci.*, 2, 32-36.
- McCormack, J. P., and S. D. Eckermann (2013), Generation of a quasi-biennial oscillation in a numerical weather prediction model using a stochastic gravity wave parameterization, manuscript in preparation.
- McCormack, J. P., S. D. Eckermann, D. E. Siskind, and T. J. McGee (2006), CHEM2D-OPP: A new linearized gas-phase ozone photochemistry parameterization for high-altitude NWP and climate models, *Atmos. Chem. Phys.*, 6, 4943-4972.
- McCormack, J. P., K. W. Hoppel, and D. E. Siskind (2008), Parameterization of middle atmospheric water vapor photochemistry for high-altitude NWP and data assimilation, *Atmos. Chem. Phys.*, 8, 7519-7532, doi:10.5194/acp-8-7519-2008.
- McIntyre, M. E. (1982), How well do we understand the dynamics of stratospheric warmings? *J. Meteorol. Soc. Japan*, 60, 37-65.

- NAS (2010), Assessment of intraseasonal and interannual climate prediction and variability, Committee on Assessment of Intraseasonal to Interannual Climate Prediction and Predictability, National Research Council, The National Academies Press, 192pp (http://www.nap.edu/catalog.php?record_id=12878).
- Thompson, D. W. J., M. P. Baldwin, and J. M. Wallace (2002), Stratospheric connection to Northern Hemisphere wintertime weather: Implications for prediction, *J. Climate*, 15, 1421-1428.
- Trenberth, K. E., and D. P. Stepaniak (2002) A pathological problem with NCEP reanalyses in the stratosphere. *J. Climate*, 15, 690-695.
- WCRP (2008), Position paper on seasonal prediction, First WCRP Seasonal Prediction Workshop, 4-7 June 2007, Barcelona, Spain, Report No. 3/2008, ICPO Publication No. 127, 23pp. (http://www.wcrp-climate.org/documents/WCRP_SeasonalPrediction_PositionPaper_Feb2008.pdf).
- Weare, B. C., C. Cagnazzo, P. G. Fogli, E. Manzini, and A. Navarra (2012), Madden-Julian Oscillation in a climate model with a well-resolved stratosphere, *J. Geophys. Res.*, 117, D01103, doi:10.1029/2011JD016247.

PUBLICATIONS

- Coy, L., and C. A. Reynolds (2013), Structure and evolution of stratospheric singular vectors during the January 2009 stratospheric sudden warming, *Quart. J. Roy. Meteorol. Soc.*, in press.
- Eckermann, S. D. and J. P. McCormack (2013), Extension of linearized parameterizations of gas-phase stratospheric ozone photochemistry through the upper stratosphere, mesosphere and lower thermosphere, (paper in preparation).
- Eckermann, S. D., J. P. McCormack, J. Ma, T. F. Hogan, and K. A. Zawdie (2013), Stratospheric analysis and forecast errors using hybrid and sigma coordinates, *Mon. Wea. Rev.*, (in press).
- Hogan, T., M. Peng, N. Baker, C. Reynolds, B. Ruston, M. Liu, J. Ridout, S. Eckermann, J. Moskaitis, T. Whitcomb, K. Viner, J. McLay, P. Pauley, L. Xu., R. Langland, M. Flatau, J. McCormack, and S. Chang (2013), The Navy Global Environmental Model, *NRL Review 2013*, in press.
- Hoppel, K. W., S. D. Eckermann, L. Coy, G. E. Nedoluha, D. R. Allen, S. D. Swadley, and N. L. Baker (2013), Evaluation of SSMIS upper atmosphere sounding channels for high-altitude data assimilation, *Mon. Wea. Rev.*, 141, 3314-3330.
- McCormack, J. P., and S. D. Eckermann (2013), Generation of a quasi-biennial oscillation in a numerical weather prediction model using a stochastic gravity wave parameterization, manuscript in preparation.

HONORS/AWARDS/PRIZES

1. Stephen Eckermann received the 2013 Sigma-Xi Award for Applied Science from the NRL Edison Chapter for foundational contributions to the Navy's high-altitude forecasting and analysis capabilities.
2. Stephen Eckermann was awarded the 2013 American Meteorological Society's Editor's Award of the *Journal of the Atmospheric Sciences* for "thorough and detailed reviews with well-informed,

well-posed and carefully argued questions for authors”: see
<http://www.ametsoc.org/awards/2013awardrecipients.pdf>

3. Stephen Eckermann was one of ten NRL awardees of the Navy Acquisition Excellence Award for Technology Transition, for the Navy Global Environmental Model (NAVGEN): see
<http://www.nrl.navy.mil/media/news-releases/2013/nrl-receives-navy-acquisition-excellence-award-for-global-weather-prediction-model>